Inversion of Satellite Ocean-Color Data

Robert Frouin

Scripps Institution of Oceanography
La Jolla, California, USA

ADEOS-2 AMSR/GLI Workshop,Tsukuba, Japan, 30 January 2007

Collaborators

Pierre-Yves Deschamps, University of Lille

Hajime Fukushima, Tokai University

Lydwine Gross-Colzy, Capgemini, Toulouse

Hiroshi Murakami, EORC, JAXA

Takashi Nakajima, Tokai University

Bruno Pelletier, University of Montpellier

Linear combination of TOA reflectance

Principle of the Method

-The top-of-atmosphere reflectance in selected spectral bands is combined linearly, after correction for molecular scattering and sun glint contributions.

-The coefficients of the linear combination minimize the perturbing effects, due to scattering and absorption by aerosols, and reflection by the surface. These effects are decomposed into a polynomial or principal components.

-The spectral bands are selected so that the linear combination is sensitive to chlorophyll-a concentration.

Minimization of Perturbing Effects

-TOA reflectance

$$R_{TOA}(\lambda) = R_m(\lambda) + R_a(\lambda) + R_{ma}(\lambda) + T_m(\lambda)T_a(\lambda)R_w(\lambda)$$

$$R_c(\lambda) = R_{TOA}(\lambda) - R_m(\lambda) = R_a(\lambda) + R_{ma}(\lambda) + T_m(\lambda)T_a(\lambda)R_w(\lambda)$$

$$= R'(\lambda) + T_m(\lambda)T_a(\lambda)R_w(\lambda)$$

-Linearly combining the corrected reflectance R_c in spectral bands centered at λ_i yields the index

$$I = \Sigma_i [a_i R_c(\lambda_i)] = \Sigma_i [a_i R'(\lambda_i)] + \Sigma_i [a_i T_m(\lambda_i)T_a(\lambda_i)R_w(\lambda_i)]$$

-To eliminate most of the atmospheric influence on I, one has to find coefficients a_i that fulfill

$$\Sigma_i [a_i R'(\lambda_i)] = 0$$

-For this, $R'(\lambda_i)$ is decomposed in a polynomial or principal components, i.e.,

$$R'(\lambda_i) \approx \Sigma_j [b_j e_{ji}]$$

-In general, a satisfactory representation can be obtained with only a few eigenvectors, e_j, since R' is a smooth function of wavelength.

-Substituting R' by its linear expression, we obtain

$$\Sigma_i \{[a_i \ \Sigma_j [b_j e_{ji}]\} = \Sigma_j \{[b_j \ \Sigma_i \ a_i e_{ji}]\} = 0$$

-To satisfy this equation, it is sufficient to have, for each e_j

$$\Sigma_i [a_i e_{ji}] = 0$$

-This system of linear equations is solved using *p* wavelengths, $n = p-1$ eigenvectors, and $a_1 = 1$.

-Note that the coefficients b_j, which vary with geometry and geophysical conditions do not need to be known.

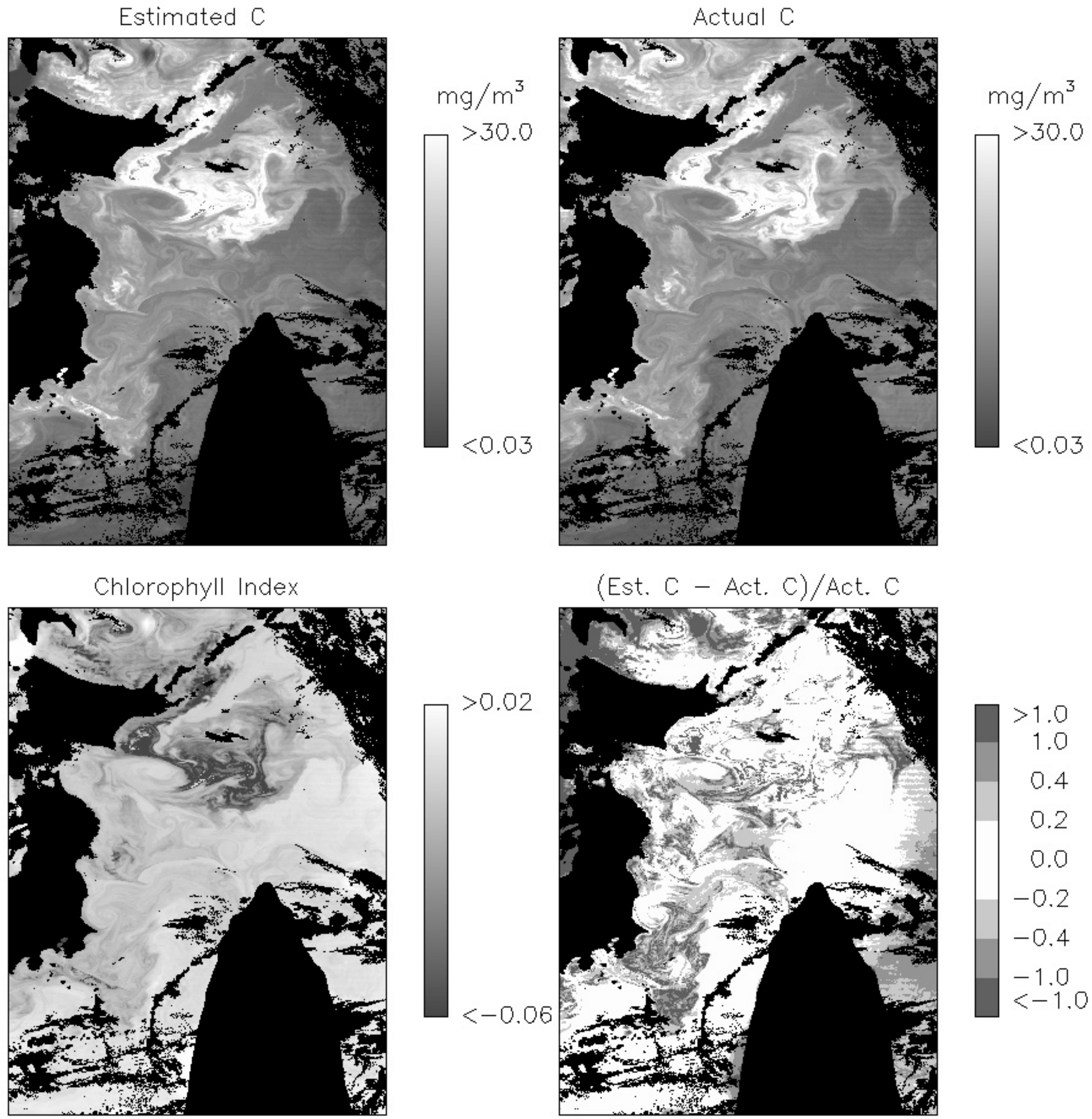

Figure 1. Application of the linear combination method to simulated GLI imagery. Perturbing effects are expressed as a polynomial.

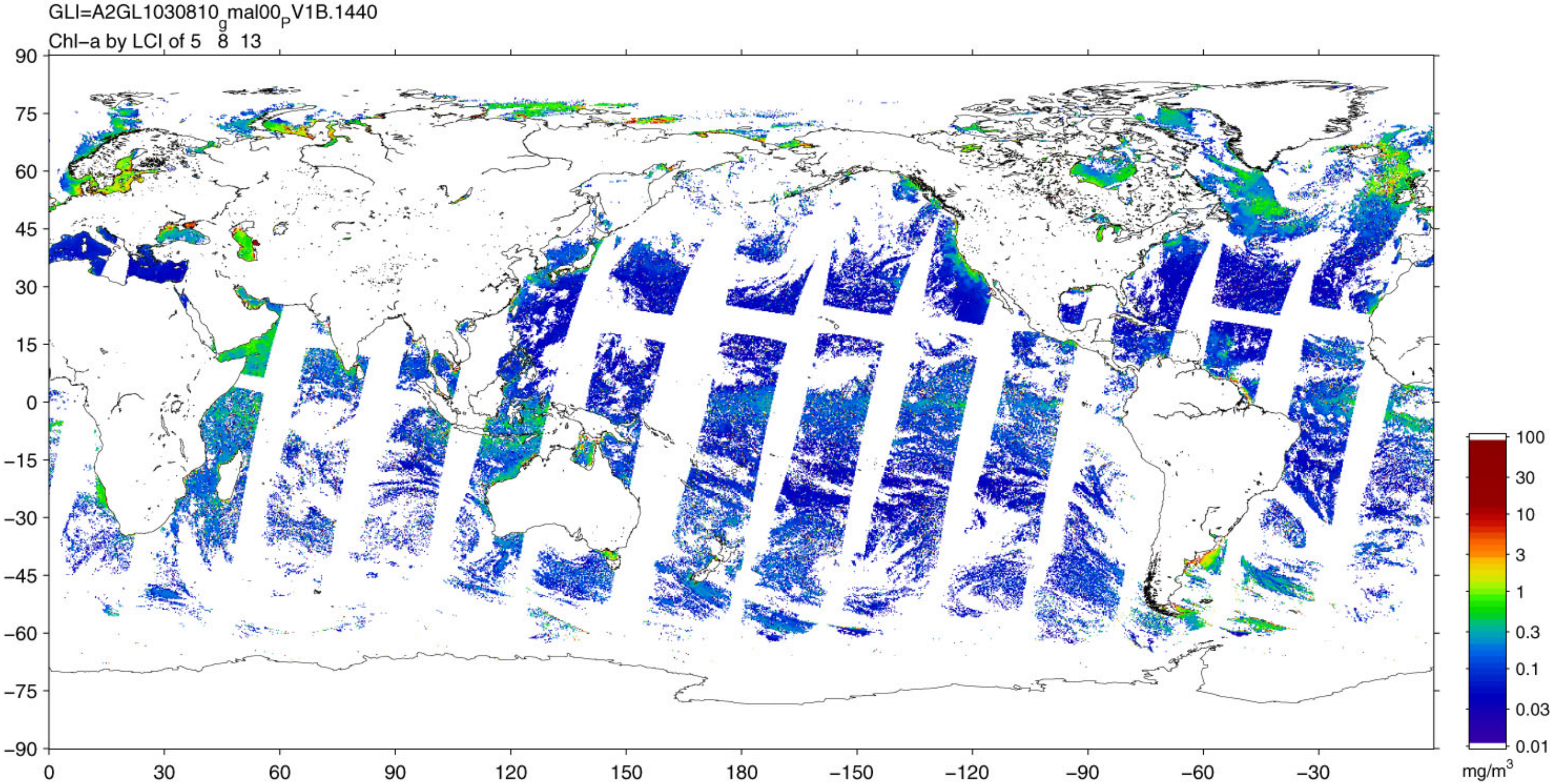

Figure 2. Application of the linear combination method to global GLI data. (Courtesy of H. Murakami, JAXA.)

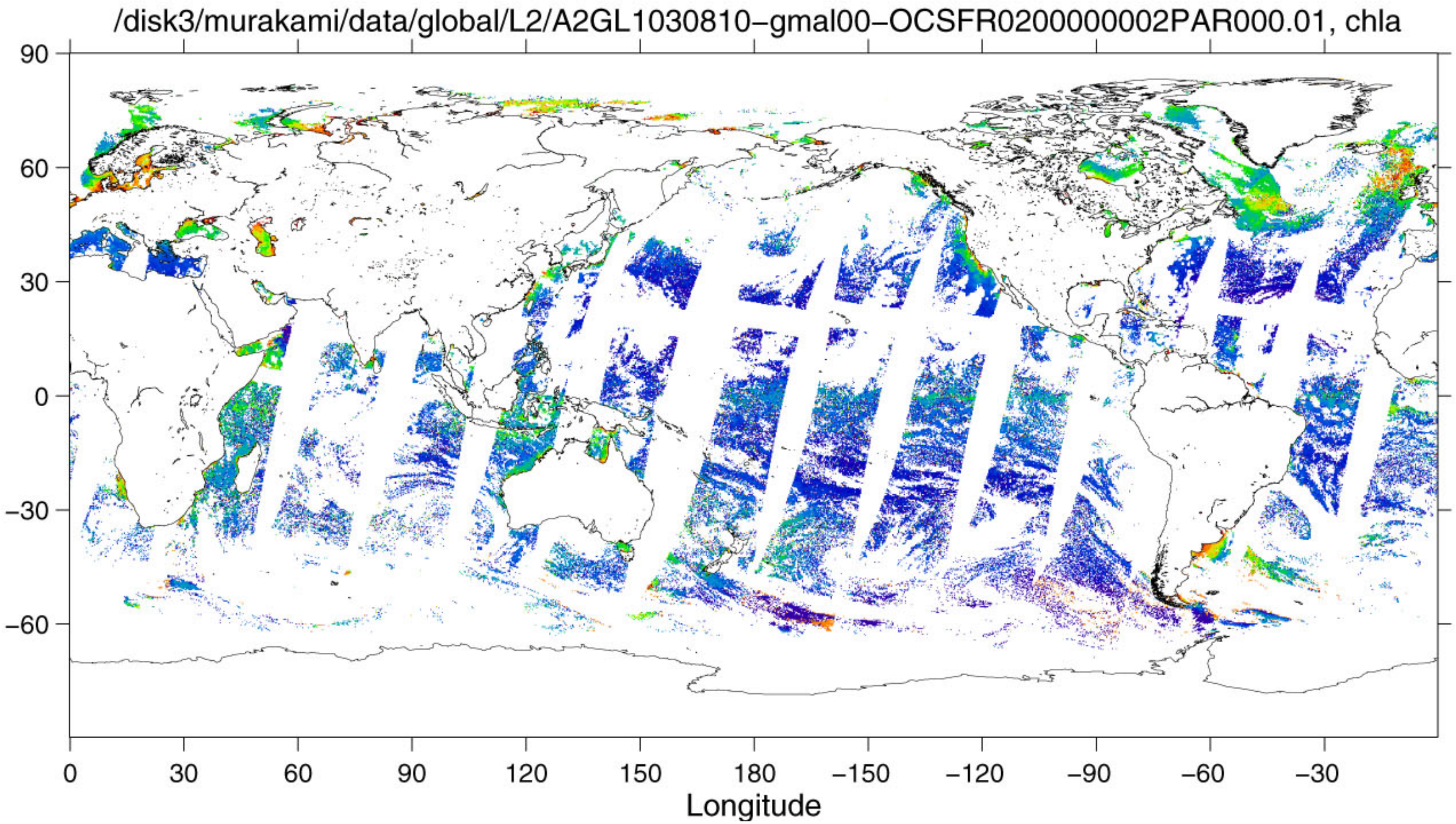

Figure 3. GLI Version 2 chlorophyll-a concentration product. (Courtesy of H.Murakami, JAXA.)

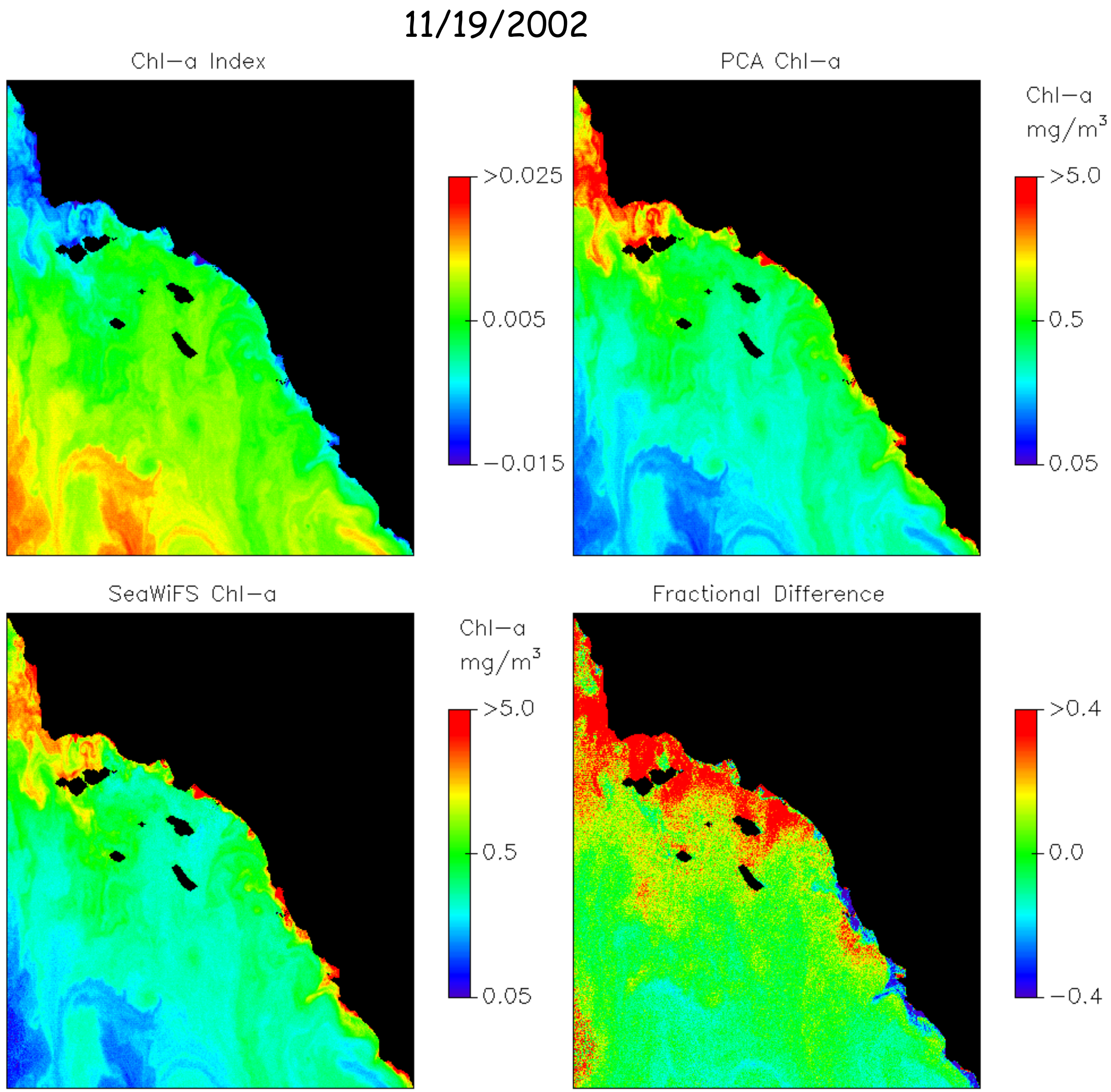

Figure 4. Application of the linear combination method to SeaWiFS imagery. The perturbing effects are decomposed into principal components.

Retrieval of the Ocean Signal

-First, a set of spectral bands is selected in the red and near infrared, for which the water body can be considered black, except in one of the spectral bands.

-Second, other sets of spectral bands are selected, that progressively include shorter wavelengths. At each step, only marine reflectance in one spectral band is unknown and therefore estimated.

$$[\lambda_i\ , i = 1, 2, \ldots, 8] = [412, 443, 490, 510, 555, 670, 765, 865]$$

$$1:\ T_m(\lambda_6)T_a(\lambda_6)R_w(\lambda_6) \approx \Sigma_i\, [a_i R_c(\lambda_i)]\ , i = 6, 7, 8$$

$$2:\ T_m(\lambda_5)T_a(\lambda_5)R_w(\lambda_5) \approx - a_6 T_m(\lambda_6)T_a(\lambda_6)R_w(\lambda_6) + \Sigma_i\, [a_i R_c(\lambda_i)]\ , i = 5, 6, 7$$

.

.

.

$$6:\ T_m(\lambda_1)T_a(\lambda_1)R_w(\lambda) \approx - a_2 T_m(\lambda_2)T_a(\lambda_2)R_w(\lambda_2) - a_3 T_m(\lambda_3)T_a(\lambda_3)R_w(\lambda_3) + \Sigma_i\, [a_i R_c(\lambda_i)]\ , i = 1, 2, 3$$

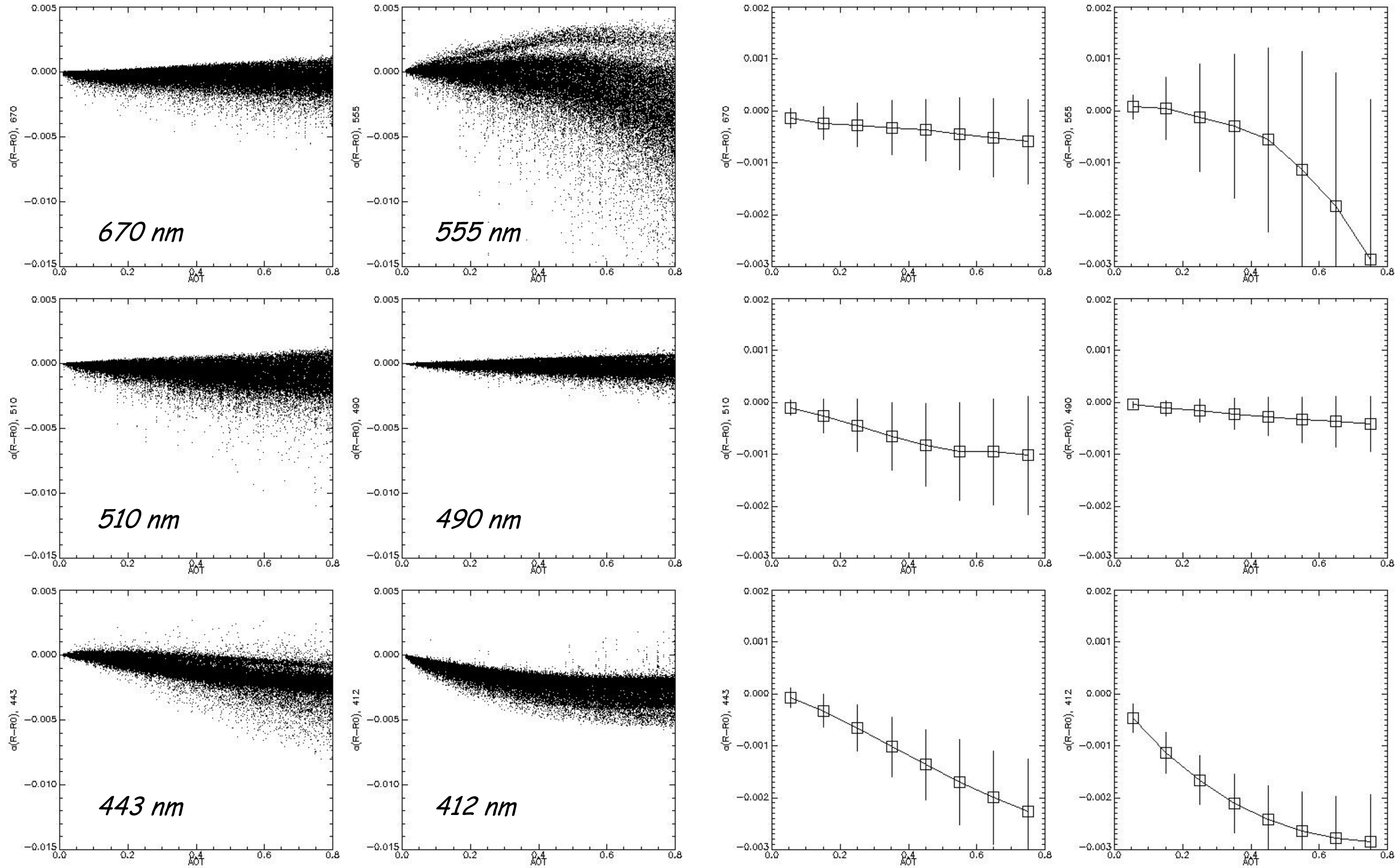

Figure 5. Residual perturbing effects of the atmosphere and surface, i.e., $\Sigma_i [a_i R'(\lambda_i)]$, as a function of aerosol optical thickness at 555 nm.

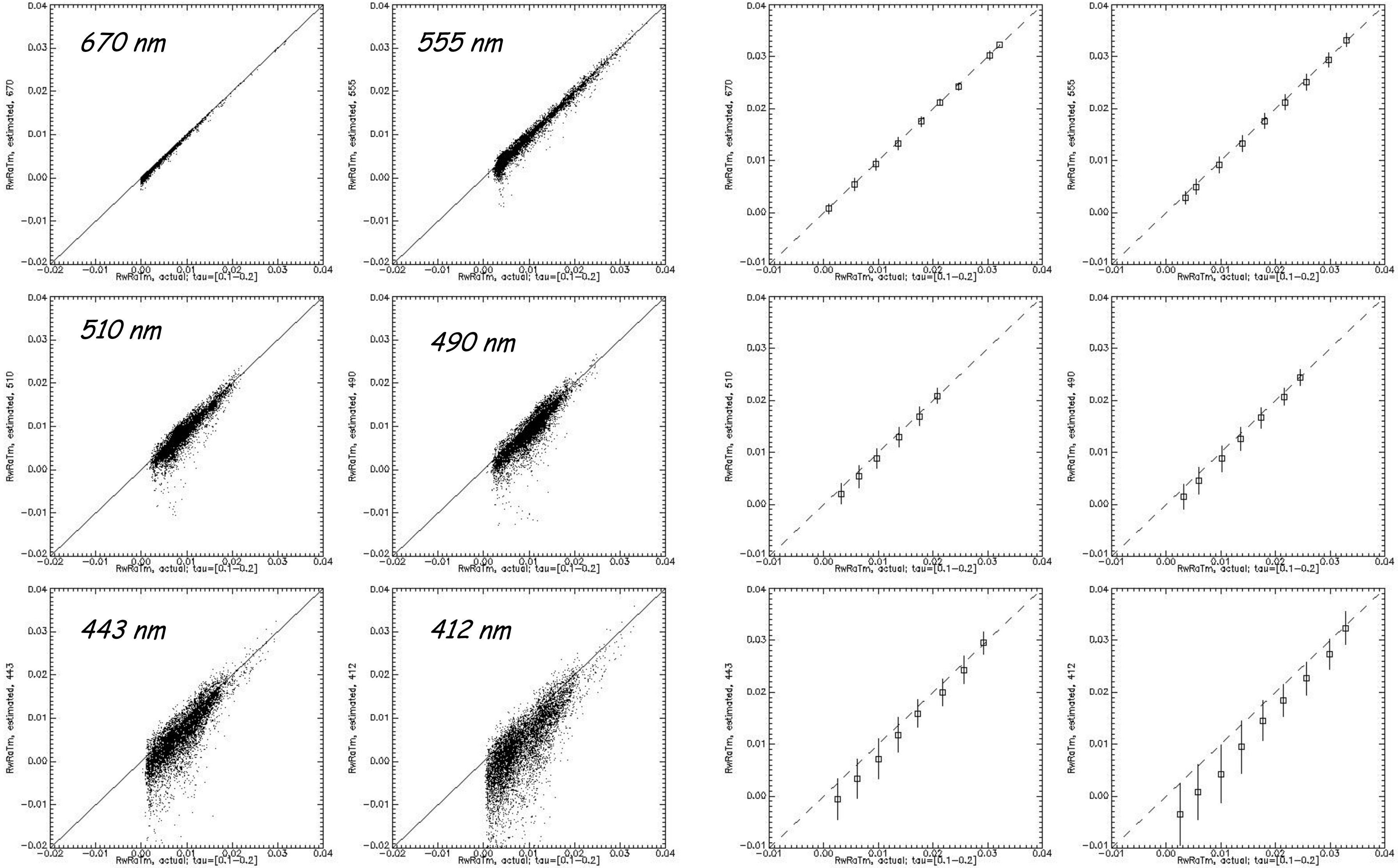

Figure 6. Comparison of estimated and actual ocean signal, i.e., $T_m(\lambda)T_a(\lambda)R_w(\lambda)$, when the optical thickness at 550 nm is between 0.1 and 0.2.

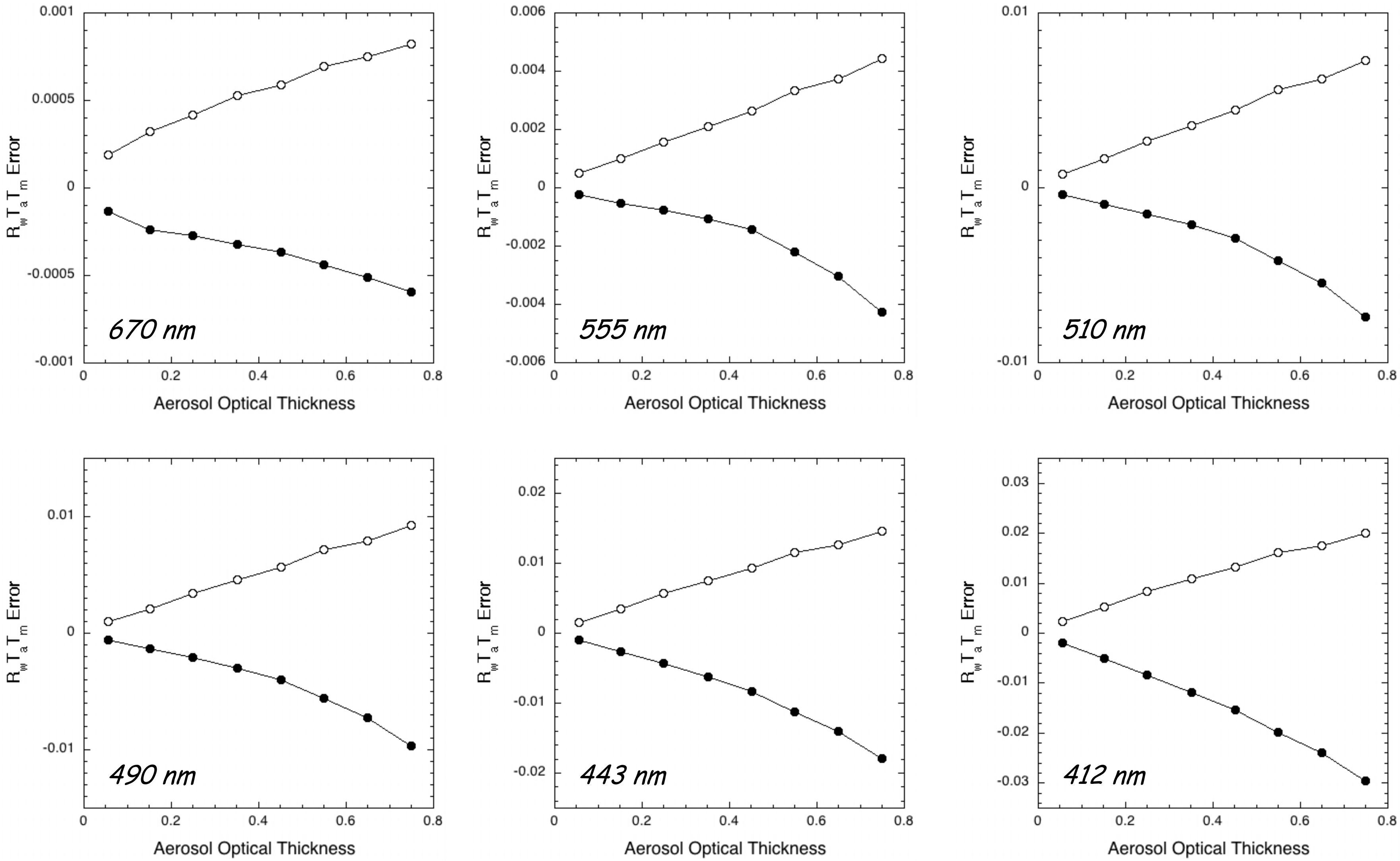

Figure 7. Performance statistics for the retrieval of $T_m(\lambda)T_a(\lambda)R_w(\lambda)$. Bias (solid circles) and standard deviation (open circles) are given as a function of aerosol optical thickness at 550 nm.

Conclusions

-The perturbing influence of the atmosphere and surface is minimized adequately for each set of wavelengths, except when aerosol loading is large. The residual effects exhibit a bias increasing with aerosol optical thickness. The bias can be reduced by taking into account the last eigenvector of the decomposition into principal components, but just globally.

-Errors in the estimated ocean signal, i.e., $T_m(\lambda)T_a(\lambda)R_w(\lambda)$, increase with decreasing wavelength (residual effects at longer wavelengths propagate) and with increasing aerosol optical thickness. They become unacceptable when the optical thickness at 550 nm is above 0.3.

-Performance can be improved by optimizing the sets of selected wavelengths, or by using a knowledge of the aerosol optical thickness, which can be estimated from the satellite data.

Fields of Nonlinear Regression Models

Problem

To estimate marine reflectance ρ_w from top-of-atmosphere reflectance ρ_{TOA} and angular variables $\boldsymbol{t}$ without knowing the other variables $\boldsymbol{x}$ that influence the radiative transfer in the ocean-atmosphere system

Methodology

-Explanatory variables (ρ_{TOA}) are considered separately from the conditioning variables (***t***).

-An inverse model is attached to each ***t***, and the attachment is continuous, i.e., the solution is represented by a continuum of parameterized statistical models (a field of non-linear regression models) indexed by ***t***:

$$\rho_W = \zeta_t(\rho_{TOA}) + \varepsilon$$

where ε is the residual of the modeling.

Methodology (cont.)

Ridge functions, selected for their approximation properties, especially density, are used to define the statistical models explaining ρ_w from ρ_{TOA} and $\boldsymbol{t}$.

$$\zeta_{\boldsymbol{t}j}(\rho_{TOA}) = \Sigma_{i = 1, \ldots, n}\, c_{ij} h(\boldsymbol{a}_i \cdot \rho_{TOA} + b_i)$$

$$\rho_{wj} = \zeta_{\boldsymbol{t}j}(\rho_{TOA}) + \varepsilon_j$$

where $\boldsymbol{a}_i(\boldsymbol{t})$, $b_i(\boldsymbol{t})$, and $c_{ij}(\boldsymbol{t})$ are the model parameters.

Simulated Data Sets

62,000 joint samples of ρ_{TOA} and ρ_W split in two data sets, D^0_e and D^0_v, for construction and validation. Noisy versions D^1_e, D^1_v, D^2_e, and D^2_v generated, by adding 1 and 2% of noise to ρ_{TOA}. The noise is defined by:

$$\rho_{TOAj}' = \rho_{TOAj} + \nu^c \rho_{TOAj} + \nu^{uc}_j \rho_{TOAj}$$

where ν^c and ν^{uc}_j are random variables uniformly distributed on the interval $[-\nu/200, \nu/200]$, where ν is the total amount of noise in percent.

Function Field Construction

-The free parameters of the field, i.e., the maps $a_i(t)$, $b_i(t)$, and $c_{ij}(t)$, are estimated by multi-linear interpolation on a regular grid covering the range of t.

-The adjustment is considered in the least-square sense, and minimization of the mean squared error is carried out using a stochastic gradient descent algorithm.

Function Field Construction (cont.)

-A sufficient number of $n = 15$ basis functions was selected via simulations, and three fields of this kind, ζ^0, ζ^1, and ζ^2 were constructed for 0, 1, and 2% of noise.

-Since the components ζ_{tj} take their values in the same vector space (the vector space spanned by the linear combinations of ridge functions), the approach is not equivalent to separate retrievals on a component-by-component basis.

Theoretical Results for GLI

				Field ζ^0			
	λ (nm)	380	412	443	460	520	545
$\mathcal{D}_e^0$	RMS	0.000357	0.000362	0.000221	0.000165	$5.33e-05$	$6.64e-05$
	RMSR	0.027290	0.025008	0.019108	0.016000	$6.19e-03$	$7.69e-03$
$\mathcal{D}_v^0$	RMS	0.000357	0.000363	0.000221	0.000165	$5.36e-05$	$6.63e-05$
	RMSR	0.028168	0.025763	0.019607	0.016372	$6.23e-03$	$7.65e-03$
$\mathcal{D}_e^1$	RMS	0.000901	0.000846	0.00055	0.000422	0.000150	0.000187
	RMSR	0.055998	0.049971	0.04171	0.036165	0.016896	0.021906
$\mathcal{D}_v^1$	RMS	0.000888	0.000833	0.000543	0.000417	0.000152	0.000186
	RMSR	0.056408	0.049936	0.041885	0.036508	0.017140	0.021722
				Field ζ^1			
$\mathcal{D}_e^0$	RMS	0.000434	0.000431	0.000267	0.000202	$6.96e-05$	$8.48e-05$
	RMSR	0.028771	0.025905	0.021234	0.018443	$8.02e-03$	$9.91e-03$
$\mathcal{D}_v^0$	RMS	0.000433	0.000433	0.000267	0.000202	$7.18e-05$	$8.56e-05$
	RMSR	0.029120	0.026096	0.021457	0.018729	$8.30e-03$	$9.95e-03$
$\mathcal{D}_e^1$	RMS	0.000654	0.000631	0.000402	0.000309	$9.76e-05$	0.000132
	RMSR	0.041901	0.037426	0.031563	0.027655	$1.12e-02$	0.015271
$\mathcal{D}_v^1$	RMS	0.000646	0.000624	0.000397	0.000305	0.000100	0.000131
	RMSR	0.041971	0.037267	0.031546	0.027777	0.011457	0.015066

Table 1. Root Mean Squared error (RMS) and Root Mean Squared Relative error (RMSR) for the models ζ^0 and ζ^1 evaluated on the construction and validation data sets (D^0_e and D^0_v) and on 1% noisy versions of them (D^1_e and D^1_v).

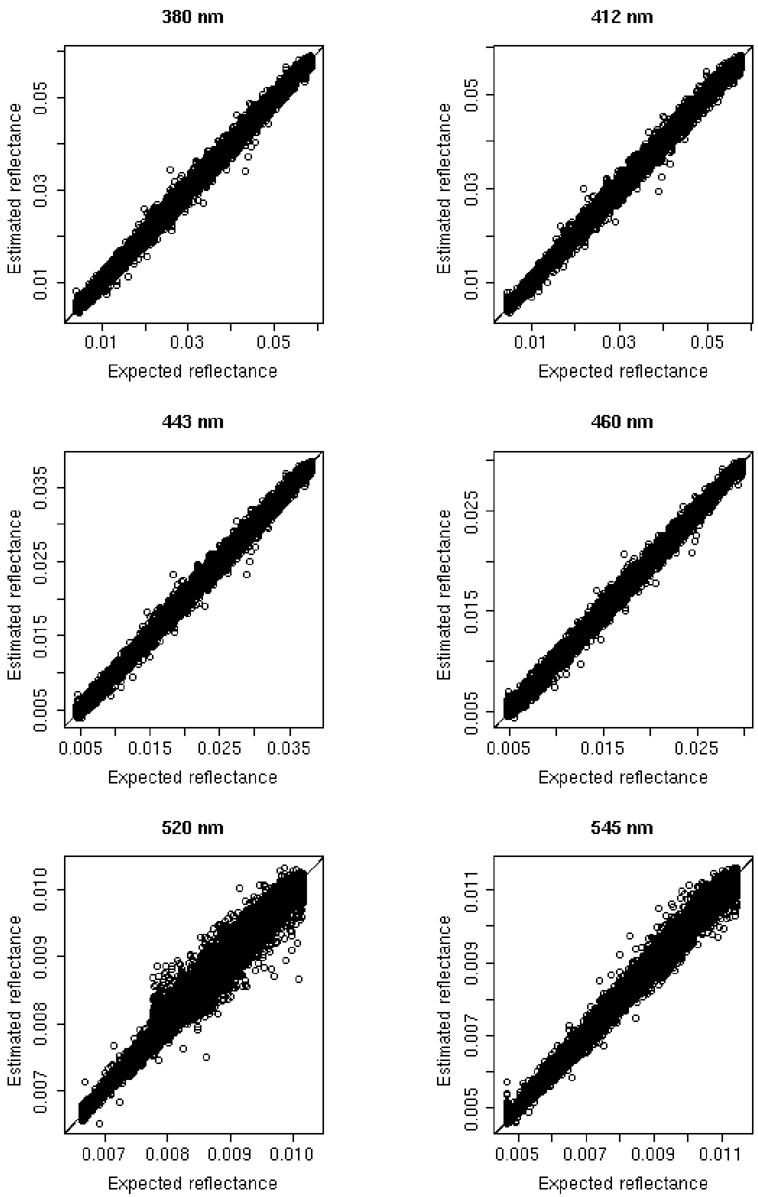

Figure 8. Estimated versus expected marine reflectance for model ζ^1 adjusted on 1% noisy data.

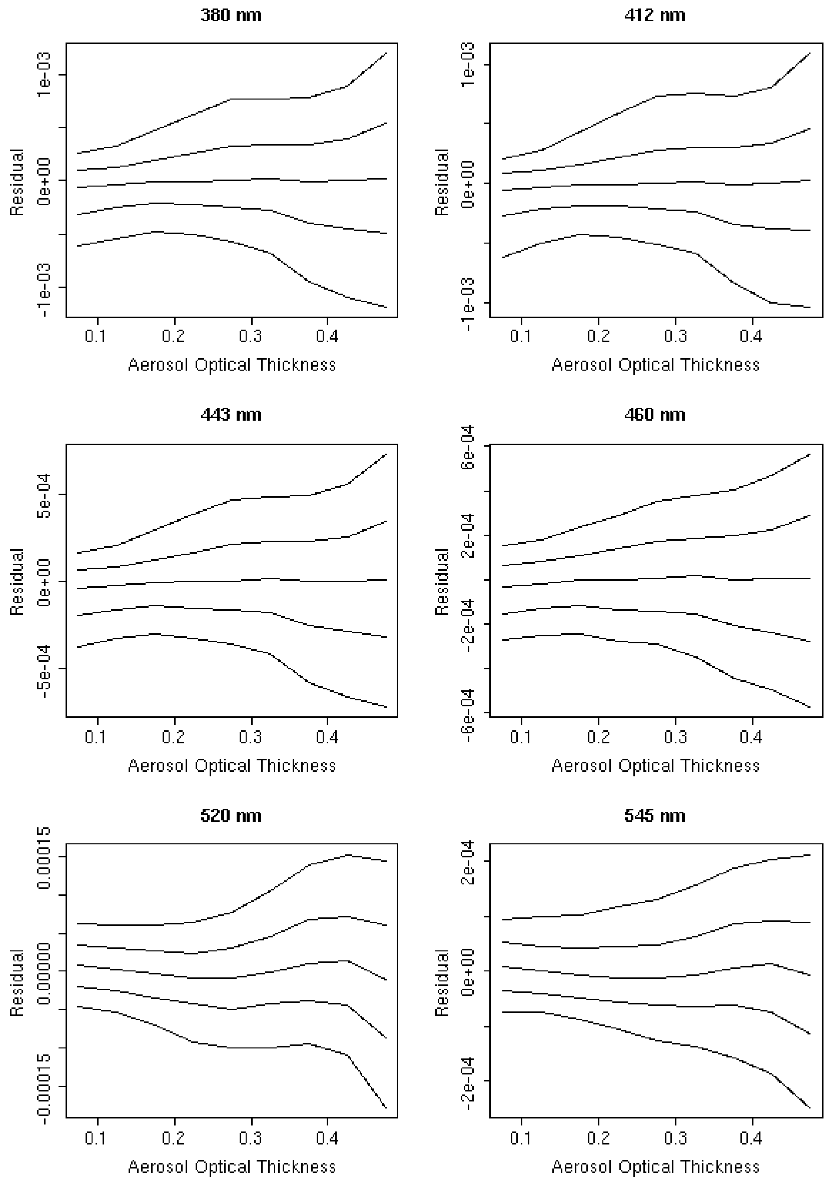

Figure 9. Conditional quantiles (of order 0.1, 0.25, 0.5, 0.75, and 0.9) of the residual ρ_w error distributions as a function of aerosol optical thickness at 550nm for model ζ^1 applied to 1% noisy data.

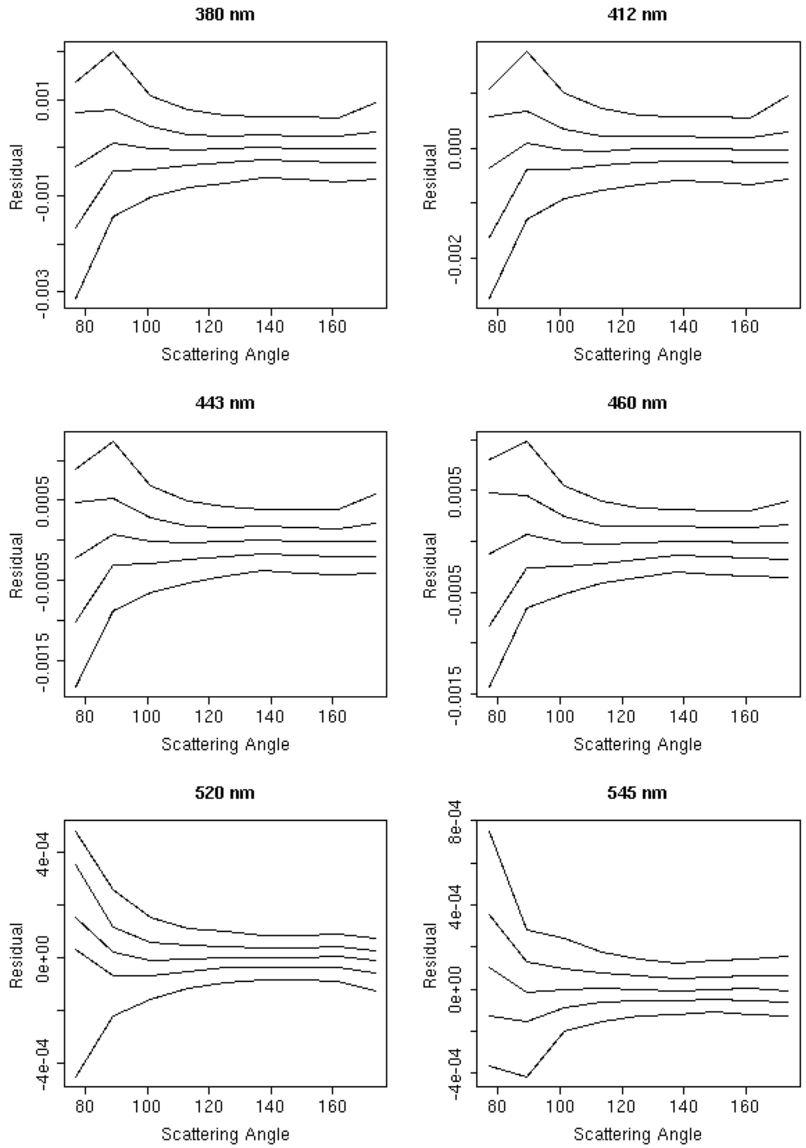

Figure 10. Conditional quantiles (of order 0.1, 0.25, 0.5, 0.75, and 0.9) of the residual ρ_w error distributions as a function of scatering angle for model ζ^1 applied to 1% noisy data.

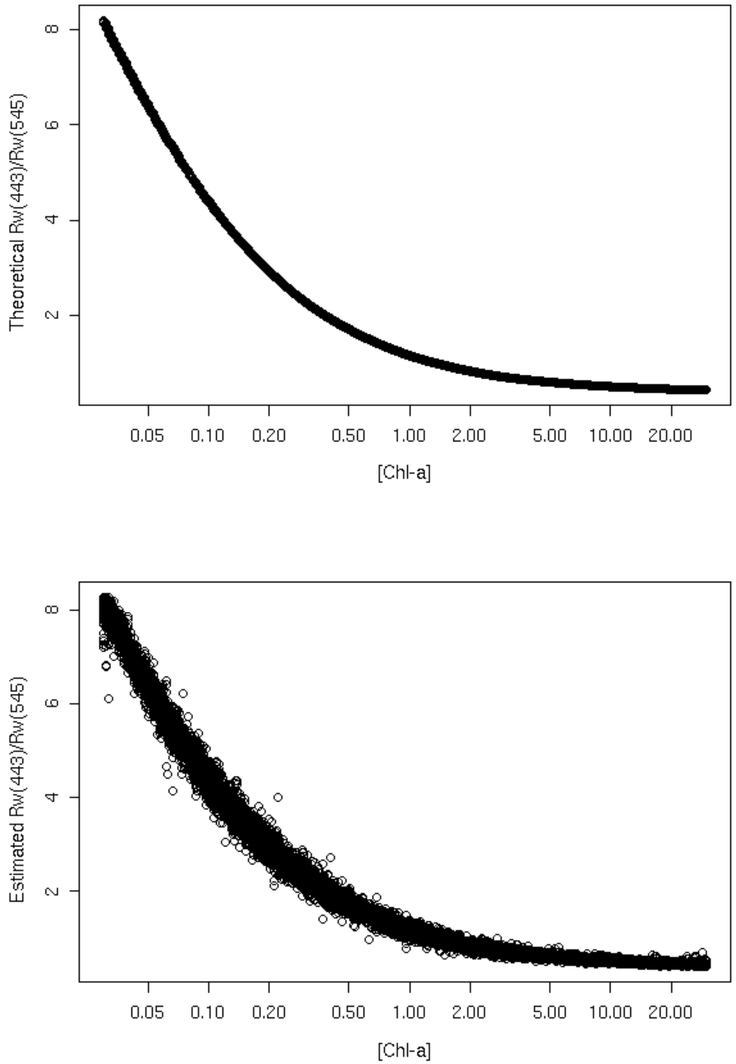

Figure 11. $\rho_w(443)/\rho_w(545)$ as a function of *[Chl-a]* for theoretical ρ_w and for ρ_w estimated by ζ^1 from 1% noisy data.

Application to SeaWiFS Imagery

-Function field methodology tested on SeaWiFS imagery acquired on day 323 of year 2002 over Southern California.

-ζ_t^2 gives large differences in ρ_w compared with SeaDAS values, resulting in 78% difference in chlorophyll-a concentration on average.

-Differences may be explained by large noise level on ρ_{TOA} (e.g., 14% at 412 nm), due to RT modeling uncertainties.

-Noise distribution estimated on 2,000 randomly selected pixels of the imagery, and introduced during the execution of the stochastic fitting algorithm, yielding function field ζ_t*.

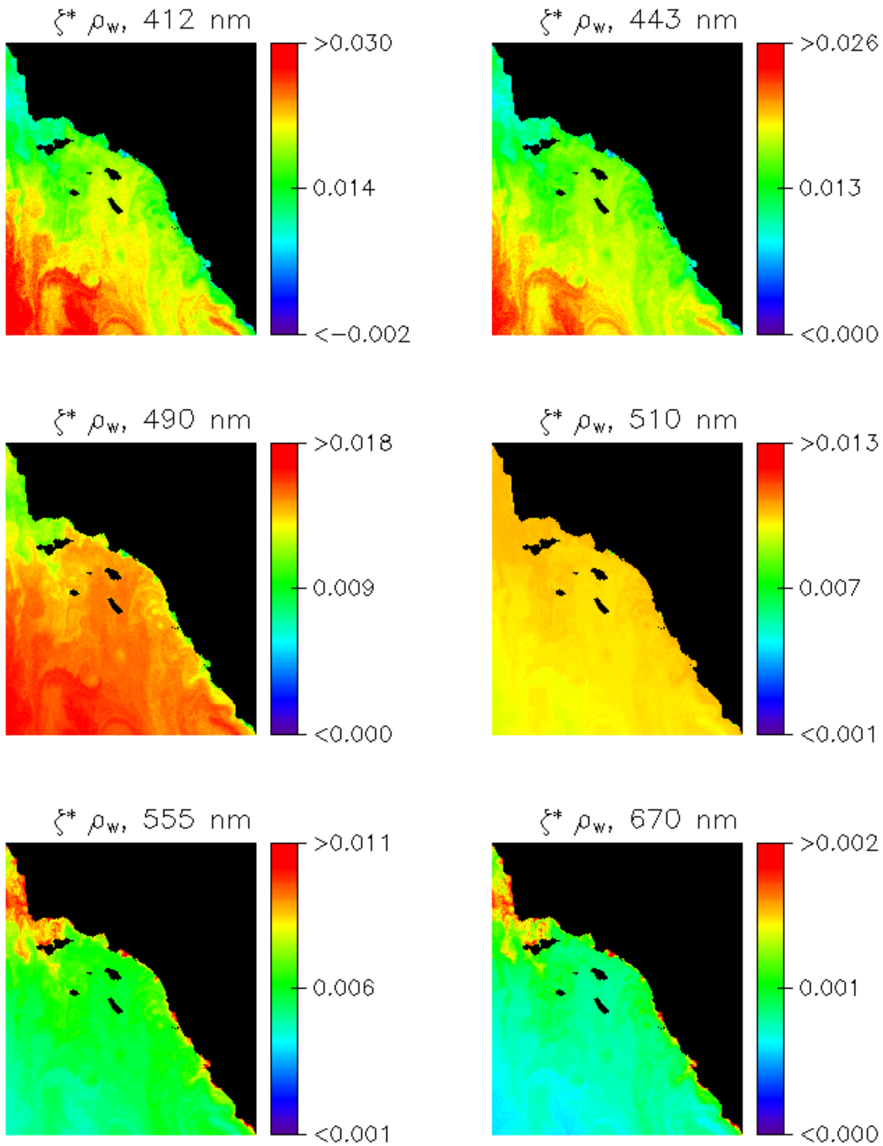

Figure 12. Marine reflectance ρ_w estimated by ζ^* for SeaWiFS imagery acquired on day 323 of year 2002 over Southern California.

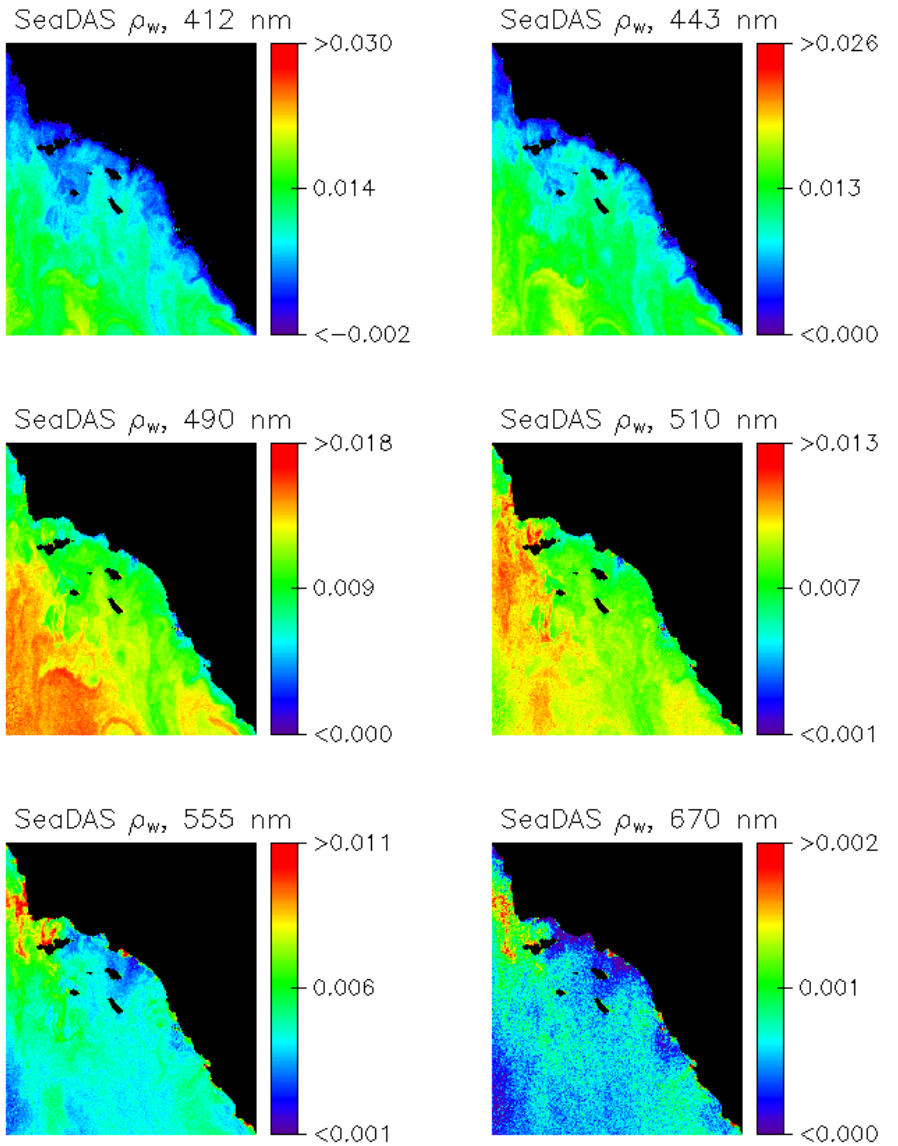

Figure 13. Marine reflectance ρ_w estimated by SeaDAS for SeaWiFS imagery acquired on day 323 of year 2002 over Southern California.

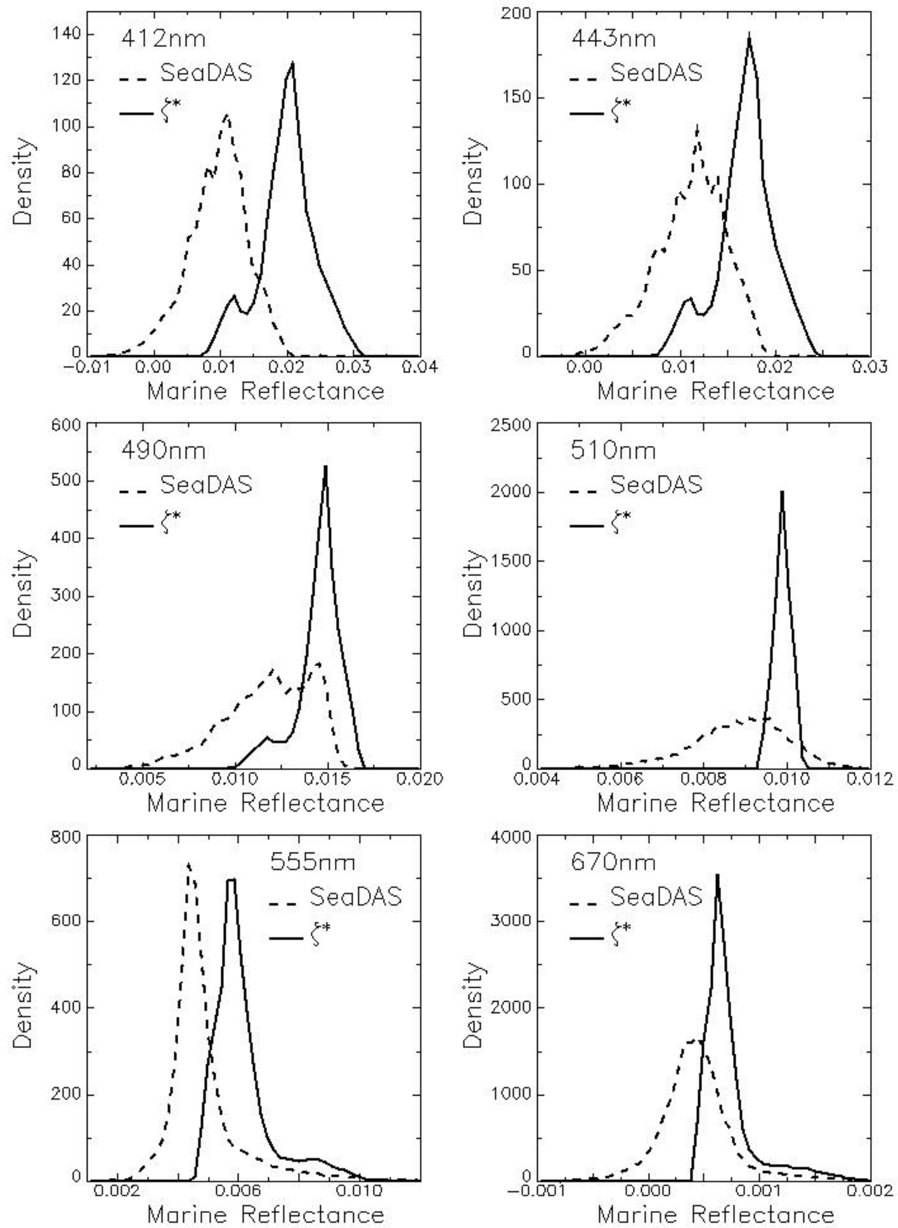

Figure 14. Histograms of marine reflectance ρ_w retrieved by SeaDAS and ζ*.

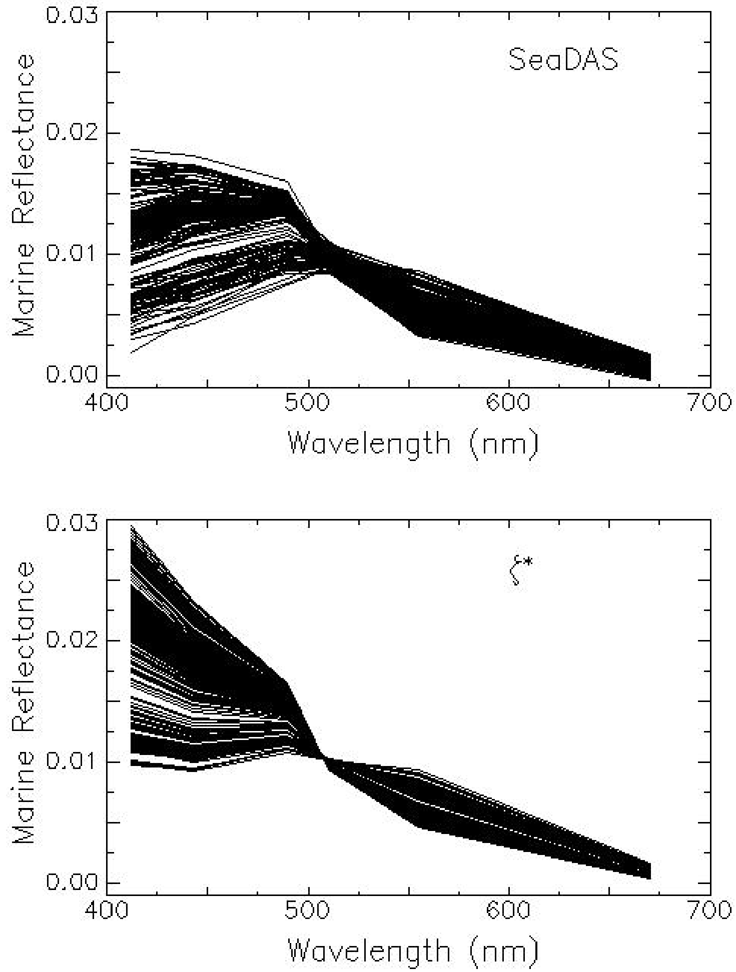

Figure 15. Marine reflectance spectra retrieved by SeaDAS and ζ^*.

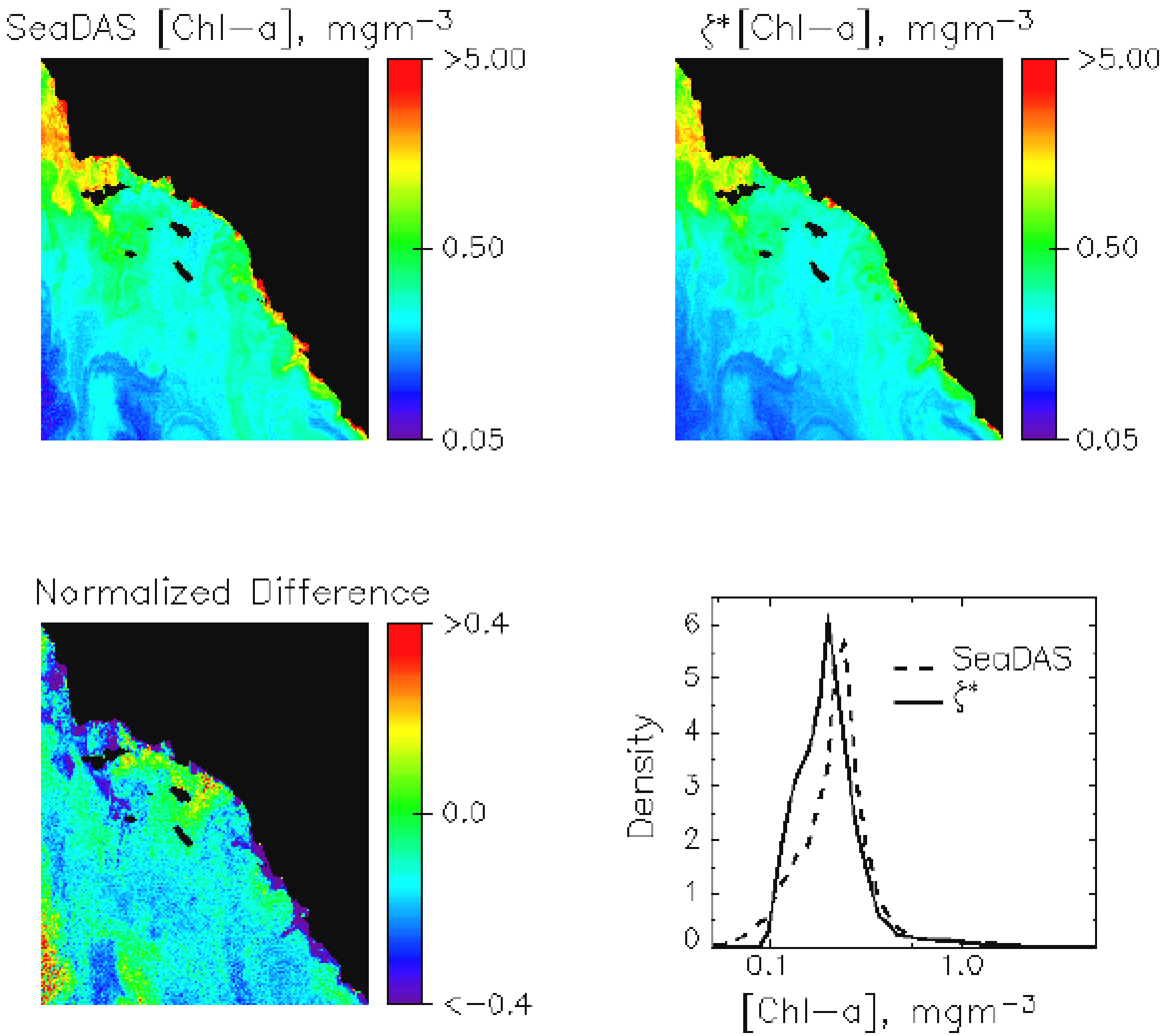

Figure 16. *[Chl-a]* retrieved by SeaDAS and ζ*, fractional difference, and histograms for SeaWiFS imagery acquired on day 323 of year 2002 over Southern California. Average difference is 19.6%.

Conclusions

Fields of non-linear regression models emerge as solutions to a continuum of similar statistical inverse problems. They match well the characteristics of the remote sensing problem, allowing separation of the explanatory variables (ρ_{TOA}) from the conditioning variables ($\boldsymbol{t}$).

The inversion is robust, with good generalization, and computationally efficient. The retrievals of ρ_w are accurate, with an error uniform over the entire range of ρ_w values. Situations of absorbing aerosols are handled well.

For noise levels up to a few percent, a general noise scheme may be appropriate, but for large noise levels, the noise distribution needs to be estimated. A plug-in approach may be reasonable.